Design and Optimization of Wheel Geometries for Enhanced Maneuverability and Resilience in Lunar Rovers

Ashira Sahunalu*, Preston Jude Wissler†, Connor Everette James‡, Lee Whaley Graber§, and Brooklyn Schnupp¶
University of Georgia, Athens, GA, 30605

Historical lunar missions have demonstrated the susceptibility of traditional rigid-wheel architectures to fatigue and structural failure when subjected to the highly abrasive lunar surface. To address these structural vulnerabilities, the objective of this study is to adapt and optimize a bio-inspired wheel architecture, leveraging camel hoof morphology and ostrich-toe tread design, with the intention of creating a robust and versatile wheel suitable for NASA rovers deployed on lunar missions. Driven by the performance metrics of the Rock and Roll with NASA challenge, this project targets three key technical benchmarks: maintaining speeds exceeding 24 km/h, achieving a lifespan capable of traversing over 1,000 km of lunar terrain, and supporting a minimum load of 256 N per wheel. To achieve these goals, the proposed design incorporates four distinct functional elements. First, the wide, flexible hoof geometry maximizes the contact surface area to prevent sinking into loose, powdery regolith, thereby enhancing maneuverability. Second, an exterior layer of biomimetic ostrich treads delivers the mechanical grip needed to scale rocky obstacles and maximize traction in loose lunar regolith. Third, an integrated, rigid eight-spoke Aluminum 6061-T6 central hub anchors the internal architecture, ensuring optimal load distribution to the rover's axle. Lastly, a seamless Ti-Al-Cr Shape Memory Alloy (SMA) exterior shell serves as the wheel's compliant mechanism, deforming to conform to uneven terrain and enhance kinetic shock absorption. The proposed wheel offers a superior method of maneuvering across lunar terrain at high speeds and mitigates lunar dust accumulation more effectively than current designs.

I. Introduction

When it comes to mobile systems for lunar exploration, it's demonstrated that the wheel is amongst the most critical elements for an effective rover (1). The flexibility of a rover's lunar wheels plays a key role in its usefulness in a lunar mission. A well-designed lunar wheel must be able to traverse rocky terrain while not getting stuck in the moon's powdery regolith (2). This is because it is very easy to slip or sink on the moon's deformable terrain (3). If these requirements are not met, a wheel will either wear down too quickly or get caught in the soil (4,5).

As NASA plans to return to the moon as part of the Artemis program, efforts to create superior and more reliable wheel designs for lunar rovers should be made. Frequently, wire mesh wheels have been used on lunar rovers (1). However, these wheels are subject to deformation and additional sinkage, with wires tending to break over prolonged periods, showcasing inefficiency and a lack of endurance (6). Another common example seen in space applications includes solid aluminum wheels. Still, these wheels are also known for their issues, including quick degradation and a potential vulnerability to getting stuck in soft sand (7). More recent examples include NASA's Spring tires. However, even these tires have yet to be tested for their ability to maintain higher speeds, with most experiments testing the wheel at only 10 km/hr (8).

With these issues in account, this project presents the design of a superior lunar wheel for NASA rovers, utilizing requirements inspired by the 2025 Rock and Roll with NASA Challenge (9). The 2025 Rock and Roll with NASA Challenge tasked participants to develop a rover wheel design that could travel over the jagged, sandy lunar surface, with the capabilities of carrying heavy loads, all while maintaining higher speeds than previously existing lunar wheels. Inspired by the premise of this challenge, this project took the following guidelines: the wheel shall be capable of supporting a minimum load of 256 N, traversing over 1000 km of lunar terrain, and maintaining speeds exceeding 24 km/hr.

*Mechanical Engineering Student, University of Georgia, AIAA Number #1923791
†Mechanical Engineering Student, University of Georgia, AIAA Number #1923760
‡Mechanical Engineering Student, University of Georgia, AIAA Number #1923958
§Mechanical Engineering Student, University of Georgia, AIAA Number #1923948
¶Mechanical Engineering Student, University of Georgia, AIAA Number #1601486

To tackle these issues, this study aims to research, implement, and test innovative rover wheel elements to design a more effective lunar wheel than previously existing designs. It was found that through four major design elements, these requirements could be met. The four major elements include a "camel hoof" wheel geometry, a tread pattern inspired by ostrich toes, a central hub interior, and a SMA exterior.

Though previous research has attempted to solve singular wheel problems and has shown promise, including speed, durability, and traction over lunar surfaces, this design intends to solve all these problems at once in a unified wheel with combined elements. The overall benefit of the paper is to test the combination of different wheel aspects to allow future rover wheels to be more effective in navigating the lunar surface.

II. Design Elements

A. Camel Hoof Design

The overall tire shape being examined in this paper resembles a camel hoof. Motivation for many aspects of the tire's design was based on biological evolutions that increase traction and reduce impact in sandy substrates. Camel hoofs have elements such as increased surface area contacting the ground and the ability to push material inward that motivate the tire design. Using a camel hoof design results in more surface area contact between the ground and the tread covering the tire, allowing increased grip in sandy terrain.

When traversing loose sand, a significant portion of the force pushed into the ground is used to push sand away. Rather than the tire gripping the sand, the sand is displaced. This means less force is pushed back into the tire to promote movement. However, a camel hoof design gives the tire the ability to push sand toward the center, allowing more grip. The sand pushed toward the center becomes compacted and provides a better surface to roll over.

According to the case study Camels and Fennec Foxes: A Case Study on Biologically Inspired Design of Sand Traction Systems (10), "The tread features a concave shape along the cross-section of the tire. The goal of this geometry was to force the soft soil sand from the edges toward the center of the tire. This action would compact the loose sand to provide an improved surface from which the tread could gain traction." The research also used a camel hoof shaped wheel, testing it through soft sand while examining slip. The camel hoof design resulted in less slip, attributed to the movement of material toward the inside of the tire. Due to this research, the camel hoof design in this paper should see similar benefits. With the inclusion of specialized tread to help bite into the terrain, further improvements are expected.

Additionally, when examining camber, the ability for a tire to maintain contact with the ground when turning allows it to maintain traction. The mechanical engineering department at California Polytechnic State University found that "maximum lateral grip is achieved at a high-negative camber angle (-40 degrees) but best longitudinal acceleration is had with no camber" (11). The camel hoof design incorporates similar slopes and angles that negative camber does to promote grip. However, it also includes spaces that allow a significant amount of tire contact when going straight, providing both neutral and negative camber benefits. It can be seen in Figure 1 that a significant portion of the force exerted on the tire results in a jacking force that can roll the tire. This paper focused on a camel hoof design to help mitigate this jacking force.

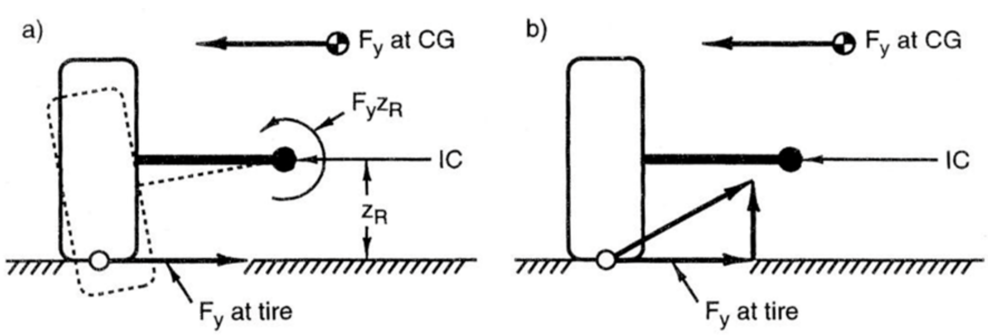

Fig. 1 Vertical jacking force due to applied lateral force, taken from Ref. 11.

B. Ostrich Toe Tread Design

Tread geometry and patterns have been a point of contention for lunar and Martian rovers for decades. From jagged spikes like that of NASA's Sojourner Rover, to a chevron pattern as seen on NASA's Curiosity Rover, tread design has gone through much trial and error over time. Expanding further on Curiosity's design, the rover's wheels have accrued much wear and tear over its 19-kilometer journey across rugged Martian terrain.

Fig. 2 MAHLI full-wheel imagery of Curiosity's left-middle wheel taken on April 18, 2016, from Ref. 12.

According to a NASA article outlining Curiosity's failures and how NASA's Perseverance rover improved on those failures (12), it explains how the holes in the rover's wheels were due to the thinnest parts of the wheels being adjacent to the points of the chevron treads. This weak point was improved in the Perseverance tread design.

In hopes of avoiding similar mistakes, this study intended to find a more durable and effective tread solution. According to a study by the Key Laboratory of Bionic Engineering at Jilin University in China (13), a tread design inspired by characteristics of an "ostrich toe" were tested against a more traditional wheel design. They coined the ostrich toe design as the "bionic wheel" and used the Discrete Element Method to test the wheels (specifically EDEM 2020). After testing elements of both wheels interchanged with regards to settlement and slip rate, they discovered that the bionic wheel has increased traction, traversing capabilities, and energy efficiency when compared to the basic wheel.

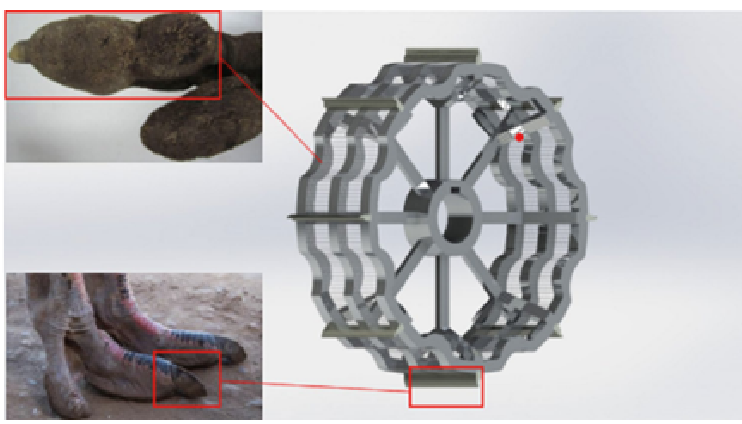

Fig. 3 3D model of bionic wheel, taken from Ref. 13.

Due to the tread pattern's clear benefits, this design incorporates a tread inspired by the bionic wheel between the grooves of the camel hoof. The tread design is intended to increase traction and durability, leading to higher traversal speeds on the lunar surface.

In terms of tread material, this study decided to use a titanium alloy, Ti-6Al-4V. According to an article on alloy (14), it is made up of 88.75–91% titanium, 5.5–6.75% aluminum, and 3.5–4.5% vanadium. It offers a low thermal conductivity of 6.7 W/mK, a high tensile strength of 1,170 MPa, and a high modulus of elasticity of 114 GPa. These characteristics make this alloy an ideal choice for this design.

C. Central Hub

An Aluminum 6061-T6 central hub anchors the core and body of this lunar wheel. Recognized as a critical aerospace material and candidate for future space exploration, this aluminum alloy was selected primarily for its favorable strength-to-weight ratio and durability (15). Exhibiting a tensile yield strength of approximately 276 MPa, Aluminum 6061-T6 provides the necessary structural integrity for the wheel's core (15). Another key benefit of using Aluminum 6061-T6 for a lunar rover wheel is its cost-effectiveness. 6061-T6 is economical, with raw materials costing generally from 2.00to5.00 per kg (16,19). According to Ref. (20), 6061-T6 acts as the 1x base cost multiplier, whereas Aluminum 7075-T6 is 2 to 3 times more expensive, and Titanium (Grade 5) is 8 to 12 times more expensive. This cost difference makes 6061-T6 the most practical in terms of strength and availability and a budget-friendly choice for the wheel's core.

Originally, the central hub was planned to be made from aluminum 7075-T6, but the decision was made to shift to aluminum 6061-T6 due to its properties. Aluminum 6061-T6 has a greater elongation rate of 12–17

The central hub holds and maintains the rover's shape and connects it to the axle via eight supporting spokes. The decision to finalize the design with eight spokes attached radially around the wheel's inner lip was based on its advantages. There are general benefits of having internal spokes. Spokes function as a secondary suspension system, mitigating loads by absorbing shocks (20). As a rover traverses rough terrain or experiences a landing event, the flexures provide a non-linear spring rate, allowing the wheel to become more compliant during high-deformation events (20). This protects the inside of the wheel hub from impact spikes. Recent engineering analyses have revealed flaws in the six-spoke architecture used by NASA's Curiosity and Perseverance rovers, suggesting that eight supporting spokes offer a superior design. A six-spoke wheel features wide, unsupported 60-degree sections around its circumference (21). Tests on flexible six-spoke wheels demonstrated that wheel stiffness fluctuates depending on whether ground contact is beneath a spoke or between two spokes (21). The disparity in stiffness causes uneven deformation as the wheel maneuvers, compromising structural integrity and movement quality. With fewer spokes, each bears more weight and stress, increasing susceptibility to failure and making it harder to maintain wheel trueness (21,22). Switching to an eight-spoke design reduces the angular gap between supports to 45 degrees, creating a "highly harmonic wheel" where stiffness and deflection remain consistent throughout a full rotation (21). The eight-spoke wheel design achieves greater deflection performance and lower resistance to motion than previous six-spoke NASA designs. By better distributing tensile loads, the eight-spoke design mitigates deformation and improves the wheel's structural integrity.

D. SMA Exterior Design

There are two major characteristics that describe the lunar surface. First, the moon's outermost layer is defined as soft, powdery regolith, a fine-grained film that is easy for a wheel to sink into and slip on. Second is the moon's rocky, uneven terrain, creating large obstacles and the potential for high impacts. A proper lunar wheel must be designed to maneuver over both these challenges while maintaining moderate speeds.

To overcome both issues simultaneously, it was determined that a deformable wheel would be optimal. Deformable wheels offer advantages over conventional rigid wheels for traversing softer terrain at moderate speeds. The wheel's ability to deform increases the surface area it has in contact with the ground. This allows the wheel to gain a boost in its grip on softer surfaces while also decreasing the pressure it applies to the ground at a point (23). This increases the wheel's traction while decreasing sinkage, making it less likely to get stuck in soft terrain. In addition, the wheel's deformability has a dampening effect on the rover, allowing it to travel across rough planetary surfaces with fewer issues compared to a rigid wheel system (23).

There are many types of deformable wheels on the market. The most common types include multimodal wheels, which switch between a highly deformable state and a solid state (24,25,26). Though beneficial for maximizing both speed and deformability, multimodal wheels also come with drawbacks. Many transition between modes using gears or mechanical systems (24,25). These systems are at increased risk of mechanical failure on the moon, where the razor-sharp regolith wears them down over time, leading to wheel failure. This, combined with the difficulty of replacing these systems in a lunar environment, makes multimodal systems undesirable for a lunar rover. Additionally, these systems often take time to switch between modes or feature a structurally compromised secondary mode (25,24). This makes the wheel suboptimal for lunar missions, as switching between modes increases travel time, counteracting the benefit of higher maximum speed.

This design proposes using an SMA material instead. A single material that can deform under pressure and return to

Fig. 4 Images of the lunar surface taken by the Chang'e 3 lunar lander and Yutu rover.

its original shape is optimal for maximizing surface area and increasing traction without the drawbacks of a multimodal wheel. The increased deformability of an SMA wheel will reduce sinkage without compromising slip ratio (23). The material chosen for the wheel's exterior was Ti-Al-Cr Shape Memory Alloy due to its resistance to temperature fluctuations, superelasticity at extreme temperatures, and reduced cost (27). This functionality at a better price made it a superior choice for the wheel exterior than the more commonly known NiTinol.

For the wheel's exterior plating, the wheel was designed with a solid sheet plate rather than the wire-mesh exterior design seen on most rover wheels. The reason for this change was to reduce sinkage into the ground. Wire-mesh wheels tend to exhibit greater sinkage compared to standard wheels (28). Given the powdery regolith that covers the moon, maintaining low sinkage was a priority. The second reason was to accommodate the addition of treads. Treads tend to pull on and break wire-mesh wires over time (29). This makes treads and wire-mesh incompatible, so a plate of material must be substituted instead.

III. Structural Design

To bring the design elements of the wheel together for the first time, a CAD model was developed. The Onshape modeling software was used due to its ease of use and collaboration features. The CAD model demonstrates how the individual design elements presented in Section II come together into one, unified functioning wheel. The wheel's outer shell and overall shape are defined by the camel hoof element described in Section II. The radius for the wheel was determined to be 9 inches. This radius was determined to closer mimic NASA's Rock and Roll guidelines.

Fig. 5 CAD wheel design.

To comply with the functionality of the SMA exterior metal, accommodate the hoof-based design, and allow for the addition of treads, a solid plate of Ti-Al-Cr SMA was used as opposed to the wire mesh design frequently seen in SMA tires. One major reason for this design choice is to allow for the addition of treads, as the presence of treads causes the wire mesh design to break over a prolonged period of time. The thickness of the SMA material varies across the wheel to provide extra support to critical areas. This thickness varies from 0.10 inches to 0.06 inches, with 0.10 inches present along edges and the middle of the wheel, and 0.06 inches alongside the surface of contact. Original designs contained upwards of 56 treads; however, this was determined to be suboptimal. The current wheel design has 28 treads in total, each evenly spaced out along its exterior. This tread frequency was chosen as additional treads would begin to hinder the SMA elements of the wheel, while fewer treads would diminish the beneficial increase in traction and velocity the treads provide. The wheel's central hub support structure is secured to the outer shell using aluminum bolts inserted through the shell and into eight designated pegs on the internal structure. For the interior supporting structure, eight spokes were chosen due to the multi-spoke alloy wheel being found to have a superior structural tendency over 6-spoke alloy wheels (30).

IV. Integration

As stated in Section III, the camel hoof design serves as the foundation for the wheel. This design was selected for its increased contact area and ability to minimize dust displacement. The increased contact area enhances traction, enabling higher speeds and superior climbing on rough terrain while preventing sinkage. The deformability of the SMA exterior further amplifies these benefits. A relatively high surface area is advantageous for our target speed range of 24 km/hr, promoting better traction, reduced sinkage, and superior terrain climbing, all critical elements on the lunar surface. A high surface area is also optimal for soft ground, a prevalent feature given the loose regolith that characterizes the moon's surface. The combination of a hoof-shaped wheel and an SMA exterior is therefore ideal, as it significantly increases the wheel's surface area without compromising the balance required for speed. Furthermore, the hoof shape's ability to minimize lunar dust displacement is also optimal, as lunar dust's electrostatically charged and highly abrasive nature necessitates minimizing its disturbance, which could become potentially hazardous at high speeds. The wheel design is then further enhanced by treads, which, combined with the wheel's deformability, provide excellent traction. This lets the wheel climb over rocks at high speeds with ease. This also increases the wheel's angular to linear momentum ratio. Finally, the interior central hub of the wheel provides enhanced structural support. It was designed with limited moving parts to mitigate wear from the razor-sharp lunar dust, which could compromise the wheel's longevity. This support allows the wheel to bear higher loads without issue, ensuring it can support the weight of the rover.

In Section I of our article, the project outlined three main goals: to bear a load of 256 N, be capable of traversing over 1000 km, and be capable of exceeding 24 km/hr. Thanks to the hoof-shaped wheel, SMA deformable aspects, and addition of treads, this wheel is capable of exceeding 24 km/hr while going through both soft-deformable ground and rocky uneven terrain. In addition, the materials chosen and the ease of which it goes over obstacles allow it to traverse large distances without wear. Finally, the interior support of the central hub allows the wheel to bear and support high weight without issue.

V. Testing and Analysis

A. Simulation 1

To validate the structural and thermo-mechanical integrity of the lunar wheel, a series of static structural simulations were conducted using Ansys. The primary objective of these simulations was to determine the stress and strain distribution, as well as the deformation behavior of the wheel when subjected to the rover's static weight load. The simulations were conducted to test the effects of the 256 N force load exerted by the rover per wheel (1024 N total) and to assess whether the CAD design and the selected material, aluminum 6061-T6, can withstand the required operational force.

The simulation included two primary boundary conditions to accurately mimic the mounting of the axle from the rover to the central hub of the wheel design. A remote force of 256 N was applied directly to the central hub of the wheel. This force is meant to simulate the downward gravitational and mechanical force exerted by the rover's axle onto the wheel's core. A fixed support was then assigned to the end of each spoke (connections) to isolate and enhance the effectiveness of the simulation on the central hub. A sample of the setup for static structural analysis can be seen in Figure 6.

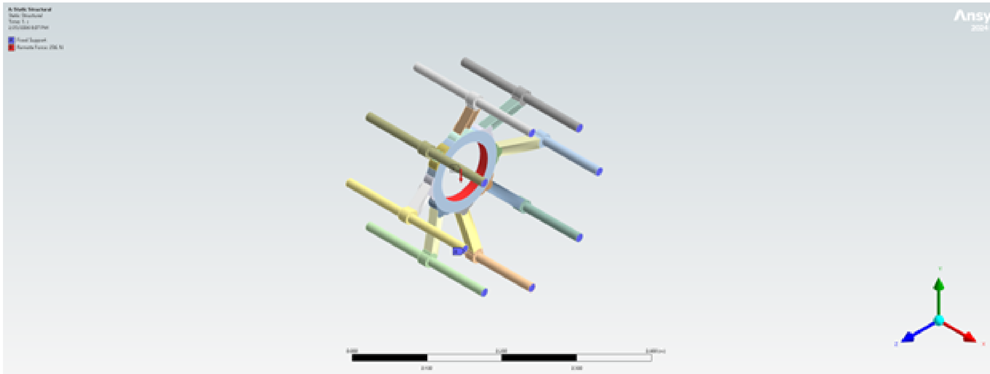

Fig. 6 Simulation setup showing remote load and fixed supports applied.

Because the lunar surface lacks an atmosphere to be able to regulate heat, a critical component of this analysis was to test the wheel material under temperature extremities experienced on the moon. Two primary thermal conditions were established using Ansys to measure the performance and the resistance of materials selected under lunar sun exposure. Test 1 introduces a cryogenic thermal condition of -130°C, experienced during the lunar night or in shadowed regions. This test ensures that the central hub, made of aluminum 6061-T6, does not become brittle under extreme temperatures and fail under load. Conversely, Test 2 is conducted at a maximum thermal condition of 120°C, simulating the extreme heat under direct solar radiation. This high-temperature analysis is critical for evaluating the aluminum 6061-T6 hub (known for thermal softening at extreme temperatures (30) to determine if it retains sufficient yield strength to support the 256 N load without extensive deformation.

Table 1 Test 1 at temperature of -130°C.

Metric	Maximum	Minimum
Total deformation	2.2825e-5 m	0 m
Equivalent elastic strain	0.00010217 mm	6.4082e-8 mm
Equivalent stress	6.6752e6 Pa	1972.8 Pa

Table 2 Test 2 at temperature of 120°C.

Metric	Maximum	Minimum
Total deformation	2.2509e-5 m	0 m
Equivalent elastic strain	0.00027614 mm	1.4561e-7 mm
Equivalent stress	1.8726e7 Pa	6083.6 Pa

B. Simulation 1: Analysis

Primarily, the indicator of most concern for the central hub's survivability is the Equivalent Stress generated by the 256 N force. In the extreme cold and hot temperatures, the simulation recorded a maximum localized stress of 6.6752e6 Pa (approx. 6.675 MPa) and 1.8726e7 Pa (approx. 18.726 MPa), respectively, along the eight-spoke aluminum 6061-T6 geometry. Correspondingly, the maximum Equivalent Elastic Strain reached only 1.0217e-4 mm and 2.7614e-4 mm, respectively, indicating that the stretching of the material is microscopic and remains within aluminum 6061-T6's elastic limits. Aluminum 6061-T6 has a maximum tensile strength of 301 MPa. Under extreme cold and hot conditions, it experiences maximum strains of 6.675 MPa and 18.726 MPa, respectively, indicating that the material can withstand applied forces exceeding 256 N. Factor of Safety (FoS) for the extreme cold and heat are 45.09 and 16.07 respectively.

While the simulation proves that the peak structural response to the 256 N load is identical in both temperature extremes, the minimal responses provide crucial insight into the wheel's long-term fatigue life. The minimum values in question can represent the baseline state experienced by the entirety of the wheel's geometry. In the cryogenic condition (-130°C), the minimum baseline for stress is 1972.8 Pa. While under direct solar radiation (120°C), stress increases to 6083.6 Pa. This indicates that the extreme heat from the sun causes greater thermal expansion, pushing outwards against the wheel's geometry more. Conversely, the minimum equivalent elastic strain is slightly higher in the extreme cold (6.4082e-8 mm) than in the extreme heat (1.4561e-7 mm). This aligns with the thermal softening of Aluminum 6061-T6, where the reduction in Young's Modulus at high temperatures makes geometry more susceptible to deformation. Because most of the volumes operate at the baseline (or minimum) levels, direct contact with solar radiation (120°C) presents a much harsher long-term operating condition than that of the cryogenic temperature (-130°C). The combination of known weaknesses to prior knowledge in Ref. 30 for thermal softening, but also the increase in strain, can lead to a greater accumulation in material fatigue, much faster than that of the 130°C cryogenic temperatures.

The total deformation metric further validates the strength and integrity of the wheel's core. Across both temperature extremities, the maximum deformation was recorded at a constant maximum of 2.2825e-5 m and 2.2509e-5 m with minimal differences along the radius of contact. This value is very small and structurally insignificant, differing from one another in such small increments, meaning that underneath a full 256 N payload, the central hub does not experience any sagging or warping. An image of the total deformation incurred is seen in Figure 7. This concludes that the core and spokes can maintain their geometry under the constant force applied.

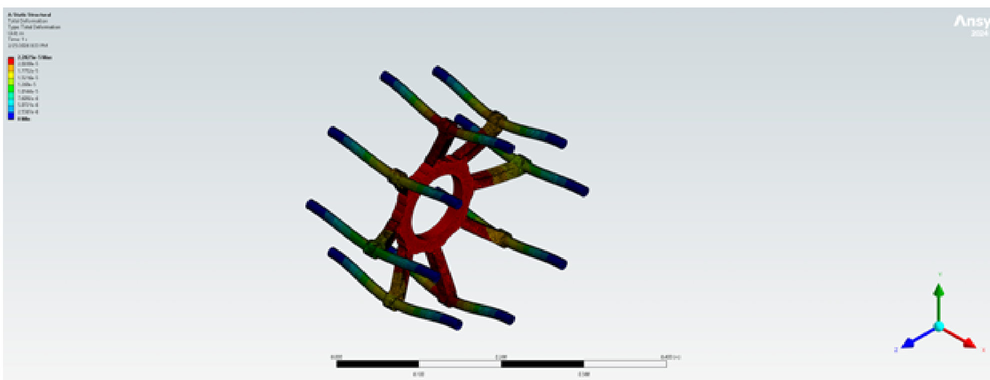

Fig. 7 Total deformation; results exaggerated.

In conclusion, the static structural, added with thermal conditions, confirms that the Aluminum 6061-T6 central hub is optimally engineered and will withstand conditions aligned with NASA's Rock and Roll Challenge. The internal ring of the central hub and eight-spoke internal can effectively withstand the 256 N force load, even with temperature extremities, validating the internal architecture of the wheel.

C. Simulation 2

For the second batch of tests, the CAD model of the wheel was ported over to the SolidWorks software. Here, using the SolidWorks' static simulation feature, the wheel was tested for its ability to absorb bumps without failure. Two forces were applied during these experiments. First, the weight of the rover was taken into account by applying a constant force of 256 N to the inner rim of the inside support structure, as shown in Figure 9. This also confirms the wheel complies with the target goal of supporting a weight of 256 N. In addition, the wheel has a constant gravity force applied to it of 1.62 m/s^2, in accordance with the moon's gravity. Next, the bump force was calculated by applying a force on a small patch upward from the bottom of the wheel (Figure 8). The magnitude of this force and the surface area of the patch it is applied to varies per experiment (Table 3 through Table 4). From the experiments, primarily stress, displacement, and safety factors were collected.

For the materials of the wheel used during simulation, the SolidWorks materials database was used. For the treads, the material selected for simulation was Ti-6Al-4V solution treated and aged (SS). For the bolts and interior support, the material selected for simulation was 7075-T6, plate (SS). Finally, for the outer shell, the material selected was X6CrNiTi18-10. This was mainly due to the SMA properties of this material providing similar results within statics tests to the material of our wheel for actual space application, that being Ti-Al-Cr SMA.

A variety of tests were run to ensure accurate results. First, the impact patch was distributed across a 60-degree angle from the center of the wheel, with the bump force kept constant at 400 N. The angle of the impact patch was then

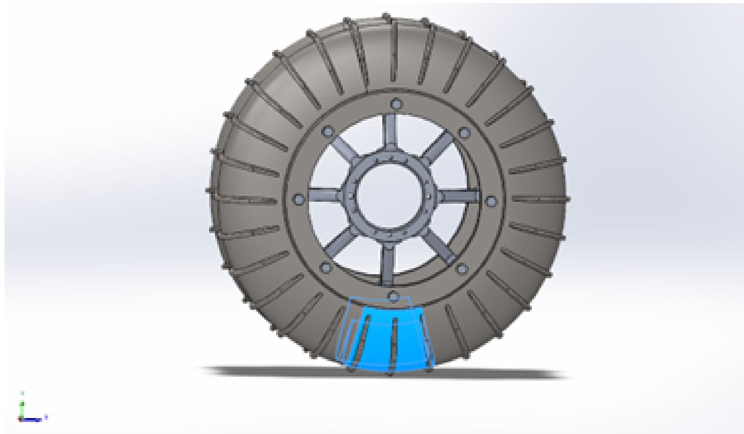

Fig. 8 SolidWorks model indicating the area the bump force is applied.

lowered to 40 degrees, 30 degrees, and 20 degrees, respectively. The results are listed in Table 3

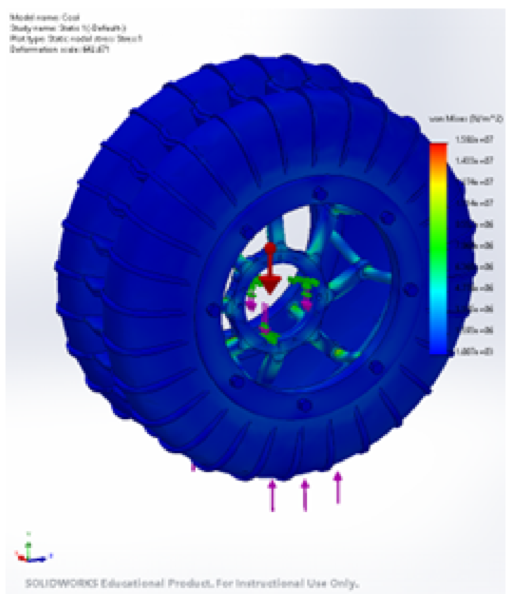

Fig. 9 SolidWorks stress simulation of an 800 N force with a 30-degree contact patch.

For the next set of experiments testing the structural integrity of the wheel when subjected to a bump force, the angle of the impact patch constant at 30 degrees while the force of the impact from the bump was altered. The following forces were tested: 400 N, 800 N, 1000 N, 1500 N, 2000 N, 4000 N, and 8000 N. The results are listed below in Table 4.

D. Simulation 2: Analysis

The goal of these experiments was to validate that the wheel could handle the forces that would result from running over bumps at high speeds. The results from Table 3 demonstrate that as long as the force being applied remains the same, no matter the area of the patch applied, the resulting effect on the wheel also remains the same. This allows us to be more confident in the results from our data as we move on to Table 4. Through testing, it was observed that the wheel could handle forces up to 8000 N while still being within an acceptable Factor of Safety ratio of 1.669. This showcases that the wheel is beyond capable of handling large impacts at high speeds, supporting claims both to having high load carrying capabilities and a long lifespan. In short, these experiments validate the stability of the wheel.

Table 3 Simulation of different contact patch angles.

Angle	Maximum stress	Minimum stress	Factor of safety
60 degrees	7.829e6 N/m^2	1.719e2 N/m^2	36.00
40 degrees	7.626e6 N/m^2	4.676e2 N/m^2	36.00
30 degrees	7.647e6 N/m^2	5.273e2 N/m^2	36.00
20 degrees	7.648e6 N/m^2	7.967e2 N/m^2	36.00

Table 4 Simulation of different bump forces.

Force	Maximum stress	Minimum stress	Factor of safety
400 N	7.647e6 N/m^2	5.273e2 N/m^2	36.00
800 N	1.592e7 N/m^2	1.007e3 N/m^2	17.27
1000 N	2.006e7 N/m^2	1.255e3 N/m^2	13.71
1500 N	3.036e7 N/m^2	2.141e3 N/m^2	9.058
2000 N	4.073e7 N/m^2	2.422e3 N/m^2	6.751
4000 N	8.209e7 N/m^2	4.864e3 N/m^2	3.350
8000 N	1.648e8 N/m^2	9.767e3 N/m^2	1.669

VI. Conclusion

This paper presents an innovative lunar wheel design for NASA rovers. It demonstrates the potential of four distinct elements: a hoof-shaped exterior, an ostrich-toe tread design, an eight-spoked central hub interior, and a shape memory alloy (SMA) exterior. By combining these elements, this paper highlights the potential of the new lunar wheel to decrease sinkage and increase traction, enabling it to meet project goals of reaching speeds of 24 km/hr, achieving a lifespan of 1000 km, and being capable of supporting a load of 256 N. To confirm the achievement of the project goals, this paper details the testing and analysis of the newly designed wheel, concluding that the project goals were met and that the wheel is capable of absorbing impacts with forces exceeding 8000 N. This paper posits that this newly designed wheel is suitable for adoption into future generations of NASA rovers that prioritize high speed and longevity.

References

[1] Asnani, V., Delap, D., and Creager, C., "The development of wheels for the Lunar Roving Vehicle," NASA 0022-4898/$36.00, February 2009, doi: 10.1016/j.jterra.2009.02.005.

[2] Noble, S., "The Lunar Regolith."

[3] Xiao, W., and Zhang, Y., "Design of manned lunar rover wheels and improvement in soil mechanics formulas for elastic wheels in consideration of deformation," 0022-4898/2016 ISTVS, March 2016, doi: 10.1016/j.jterra.2016.03.004.

[4] Wall, M., "Rugged Mars has taken big bites out of the Curiosity rover's wheels (photos)," Space.com [online database], `https://www.space.com/nasa-mars-rover-curiosity-wheel-damage-photos`, February 2022.

[5] Wall, M., "NASA's Immobilized Spirit Mars Rover Passes a Year in Silence," SpaceNews.com [online database], `https://spacenews.com/nasas-immobilized-spirit-mars-rover-passes-year-silence/`, April 2011.

[6] Huang, H., Li, J., Chen, B., Wu, B., and Zou, M., "Performance evaluation of a wire mesh wheel on deformable terrains," September 2016, doi: 10.1016/j.jterra.2016.09.003.

[7] Lakdawalla, E., "Curiosity wheel damage: The problem and solutions," The Planetary Society [online database], `https://www.planetary.org/articles/08190630-curiosity-wheel-damage`, August 2014.

[8] Naghipour, P., Padula, S., and Creager, C., "Design and Analysis of Shape Memory Spring Tires for Martian and Lunar Rover Vehicles," Structures, Dynamics and Materials Conference, June 2023.

[9] Douglas, S., "Rock and Roll with NASA Challenge," https://www.nasa.gov/directorates/stmd/prizes-challenges-crowdsourcing-program/center-of-excellence-for-collaborative-innovation-coeci/rock-and-roll-with-nasa-challenge/, September 2025.

[10] Gendreau, E., Shumaker, A., Joiner, E., Griffin, A., Pritchett, A., and Karmilovich, K., "Camels and Fennec Foxes: A Case Study on Biologically Inspired Design of Sand Traction Systems," ASME 2015 International Design Engineering Technical Conferences & Computers and Information in Engineering Conference, August 2015.

[11] French, T., Roland, A., and Sluiter, M., "Camber-Car Design & Dynamics," Mechanical Engineering Department, California Polytechnic State University, 2013.

[12] Bell, M., "Premature Wear of the MSL Wheels," NASA JPL, https://llis.nasa.gov/lesson/22401, September 2017.

[13] Zhao, Y., et al., 2024 J. Phys.: Conf. Ser. 2785 012044, doi: 10.1088/1742-6596/2785/1/012044.

[14] McClements, D., "All About Titanium Alloy 6-4: Definition, History, Properties, and Applications," Xometry [online database], https://www.xometry.com/resources/materials/all-about-titanium-alloy-6-4/.

[15] Sukumaran, A., Zhang, C., Nisar, A., Rengifo, S., and Agarwal, A., "Tribological behavior of Al 6061 and Ti6Al4V alloys against lunar regolith simulants at extreme temperatures," July 2023, doi: 10.1016/j.wear.2023.205028.

[16] Langhe-industry, "Aluminum vs. Titanium: Which Lightweight Metal Wins?," https://langhe-industry.com/aluminum-vs-titanium/.

[17] Metal Supermarkets, "What are the Differences Between 6061 and 7075 Aluminum?," https://www.metalsupermarkets.com/differences-6061-and-7075-aluminum/.

[18] VMT, "Aluminum vs. Titanium: Which Metal Is Best for Your Project?," VMT Hardware [online], https://www.machining-custom.com/blog/aluminum-vs-titanium.html, June 2025.

[19] Lo, L., "Titanium vs Aluminum CNC Machining: Strength, Weight & Cost Comparison," ecoreprap.com [online database], https://ecoreprap.com/blog/titanium-vs-aluminum-in-cnc-machining/, December 2025.

[20] Gardner, N., Kellas, S., and Hamel, J., "Utilizing 3D-DIC on the Mars 2020 Rover Wheel Assembly: Test-Analysis Correlation," 2023.

[21] Grimm, C., "Concept Development and Design of a Flexible Metallic Wheel with an Adaptive Mechanism for Soft Planetary Soils."

[22] Super Team, "Spoke Count and Carbon Wheelset Durability: What Riders Need to Know," superteamwheels.com [online database].

[23] Wang, S., Zou, M., Dang, Z., Chen, B., Zhou, T., and Su, B., "Modelling of flexible metal wheels for planetary rover on deformable terrain," January 2019, doi: 10.1016/j.tws.2019.01.047.

[24] Lee, D., Kim, J., Sohn, C., Heo, J., and Cho, K., "High-load capacity origami transformable wheel," Sci. Robot. 6, eabe0201, April 2021.

[25] Tian, H., Chu, G., Zhou, B., Zhou, D., Qiao, J., and Li, L., "4D printing of direct-driven deformable wheel with multiple programmable configurations," Int. J. Extrem. Manuf. 7 035006, January 2025, doi: 10.1088/2631-7990/ada7ab.

[26] Lee, J., and Han, S., "Variable-stiffness morphing wheel inspired by the surface tension of a liquid droplet," August 2024.

[27] Song, Y., and Xu, S., "A lightweight shape-memory alloy with superior temperature-fluctuation resistance," February 2025, doi: 10.1038/s41586-024-08583-7.

[28] Huang, H., Li, J., Chen, B., Wu, B., and Zou, M., "Performance evaluation of a wire mesh wheel on deformable terrains," October 2016, doi: 10.1016/j.jterra.2016.09.003.

[29] Padula, S., "Utilizing Shape Memory Alloys for Novel, Non-Pneumatic Tire Design," NASA [online presentation], https://ntrs.nasa.gov/api/citations/20190026976/downloads/20190026976.pdf.

[30] Czerwinski, F., "Thermal Stability of Aluminum Alloys," CanmetMATERIALS, Natural Resources Canada, Hamilton, ON, August 2020, doi:10.3390/ma13153441